IOP Publishing Journal of Geophysics and Engineering
J. Geophys. Eng. 15 (2018) 1929–1942 (14pp) https://doi.org/10.1088/1742-2140/aac097

Crossline-direction reconstruction of multi-component seismic data with shearlet sparsity constraint

Chengming Liu[1,2], Deli Wang[1,3], Jing Sun[1] and Tiexing Wang[1]

[1] College of Geo Exploration Science and Technology, Jilin University, Changchun, 130026, People's Republic of China
[2] Changchun Institute of Optics, Fine Mechanics and Physics, Chinese Academy of Sciences, Changchun 130033, People's Republic of China

E-mail: liucm1991@qq.com and wangdeli@jlu.edu.cn

Received 5 January 2018, revised 11 April 2018
Accepted for publication 27 April 2018
Published 7 June 2018

Abstract

In towed-steamer marine seismic acquisition, crossline data are fairly sparse which makes crossline wavefield reconstruction very difficult. Therefore, reconstructing the sparse wavefield becomes a fundamental and crucial step in seismic processing flow. Recently, compressed sensing has provided new insights into the data recovery problem, which combines a sparsifying transform, a sampling strategy, and a sparsity promoting algorithm. Shearlet transform is provided with a fairly good sparse representation of seismic data, and is very robust in the application of seismic wavefield reconstruction. Using multi-component measurement techniques, we propose a multi-component crossline wavefield reconstruction method based on sparse shearlet constraint inversion. By combining the pressure wavefield and its crossline gradient obtained through V_y measurements, the proposed method can effectively reduce the multiplicity caused by a limited number of samples. Both synthetic and field data have demonstrated that the method proposed in this paper, compared with the traditional wavefield reconstruction method, achieves better reconstruction resolution in the case of extremely sparse samplings and effectively suppresses the aliasing effect.

Keywords: shearlet transform, multi-component, wavefield reconstruction, crossline interpolation, sparsity constraint

(Some figures may appear in colour only in the online journal)

Introduction

With limited acquisition costs, towed-steamer marine seismic acquisition has to cover wide exploration areas, and the crossline data are usually irregular and sparse. Generally speaking, the sampling space in the crossline direction is at least four times that in the inline direction. It is difficult to identify fine structures in the deep areas in the crossline direction. Meanwhile, it is also extremely difficult to reconstruct such a wavefield.

Regular seismic data reconstruction would assume that seismic events are linear and seismic wavefronts in the time-space domain are superpositions of many plane waves, so that the low-frequency information can be extrapolated to high frequency. In order to make the events closer to linearity, Chemingui (1999) and Canning and Gardner (2012) proposed the interpolation method of dip-moveout correction and azimuth moveout correction, however, this method requires extensive calculations. Currently, many data reconstruction methods are based on the Nyquist–Shannon sampling theorem (Spitz 1991, Gulunay 1996, Liu and Sacchi 2004), which requires the sampling rate be at least twice the Nyquist rate. Otherwise, aliasing will affect the data reconstruction. However, in marine seismic data acquisition, crossline sampling is usually rather sparse, and such reconstruction methods are not applicable.

[3] Author to whom any correspondence should be addressed.

The two-component streamer measuring the vertical component of particle velocity besides the pressure component has been widely discussed (Shell Oil Co. 1984, Mobil Oil Corp. 1984, Schlumberger Technology Corp. 2004) in recent years. The high-quality vertical component can decompose the pressure component into upgoing and downgoing waves, which provides a favorable tool for deghosting (Posthumus 1993), so the frequency bandwidth of the acquired seismic data can be promoted. Robertsson *et al* (2008) proposed that the crossline particle-velocity vector besides the pressure component could be included to facilitate the crossline wavefield reconstruction. Vassallo *et al* (2010) proposed multi-channel interpolation by matching pursuit, which represents the pressure data and the crossline particle-velocity data simultaneously through sinusoidal basis functions and is able to reconstruct the wavefield even with a small number of samples. Compressed sensing (Candès and Romberg 2005, Donoho 2006, Candès and Wakin 2008) enables the high-quality data to be recovered under certain conditions from a small set of linear measurements which greatly reduces the acquisition cost and provides a powerful tool for the sparse crossline wavefield reconstruction. Fourier transform has long been the sparse representation basis function of compressed sensing, but cannot accurately reflect the local features of seismic data. Despite the remarkable success in applications, wavelets are not able to provide orientation information. Fomel and Liu (2010) introduced seislet transform to characterize and compress seismic data, which is a kind of digital wavelet-like transform. Xue *et al* (2017) developed a model regularization method based on seislet transform to improve the robustness of full waveform inversion. In recent years, curvelet transform acting as sparse representations of seismic data have been widely applied (Herrmann *et al* 2008a, 2008b).

In this paper, an alternative approach named shearlet transform outperforms curvelet transform using optimal approximation for 2D data, and we demonstrate that shearlet transform would be the optimal sparse representation for the 2D 'curve-like' seismic data, without the assumption of events being linear. We describe the wavefield reconstruction problem as an image inpainting problem using shearlets in the l_1 sparsity regularization term. In order to settle the sparse crossline wavefield reconstruction, we combined the sparsifying transform and the multi-component marine seismic measurements. We show that use of both the pressure wavefield and its spatial partial derivative obtained through the crossline particle-velocity measurements facilitates wavefield reconstruction within the limited samplings. An altering iterative method was applied to reconstruct the pressure and its crossline gradient simultaneously.

Seismic data interpolation based on shearlet transform

Compressed sensing theory is a new data acquisition theory proposed based on the sparse or compressible signals. It breaks the limits of the Nyquist–Shannon sampling theorem, enabling sufficient data reconstruction under certain conditions where the sampling rate is below Nyquist, reducing the economic and time costs. Compressed sensing has been widely used in radar, remote sensing, and image processing as the three main ingredients successfully contribute to the equation of a recovery problem that is a sparsifying transform, a sampling strategy, and a sparsity promoting algorithm.

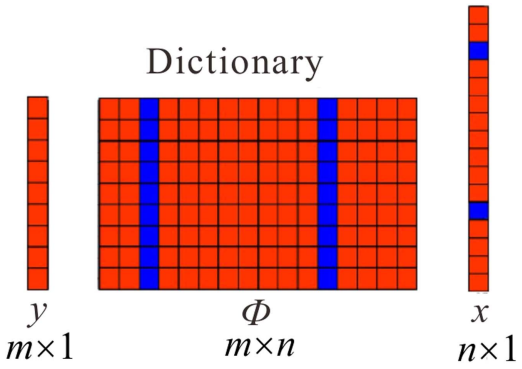

Figure 1. Compressed measurement diagram.

In a nutshell, compressed sensing measures $x \in \Re^n$ linear parts of a signal, as shown in figure 1:

$$y_k = Ax + \varepsilon_k, \ 1 < k \leqslant m, \tag{1}$$

or in the matrix:

$$y = Ax + \varepsilon, \tag{2}$$

where A is a $m \times n$ measurement matrix, m is usually smaller than n by one or several orders of magnitude, and ξ is usually the model's error term. With the compressed sensing theory, if the unknown signal x is sparse or nearly sparse, x can be reconstructed through the limited measurement data y and the measurement matrix A under some specific conditions. Generally, the above problem would be settled with the convex optimization algorithm:

$$\min_{\hat{x} \in \Re^n} \|\hat{x}\|_1 \text{ subject to } \|A\hat{x} - y\|_2 \leqslant \varepsilon. \tag{3}$$

Here, $\|\cdot\|_2$ is the 2-norm, while $\|\cdot\|_1$ is the 1-norm, ε^2 is the upper limit of noise energy, and the hat symbol $\wedge$ is reserved for estimates found through optimization. There are many methods for solving the above problem, such as orthogonal matching pursuit and the iterative threshold method (Daubechies *et al* 2004, Elad *et al* 2005), but the basis of the above method is signal sparsity. However, signals in nature are generally not sparse. We can transform the signals into various domains (e.g. Fourier, wavelet, curvelet, etc) to obtain a set of sparse coefficients. If most of the transformation coefficients of the signals are sufficiently small, and only a few have large values describing the signals, we believe the signals are sparse as well. Figure 2 shows a 35 Hz sinusoidal signal, which is obviously not sparse in the time domain but becomes extremely sparse in the Fourier domain.

With special sparsifying transform, we can represent the signal with a dictionary D (wavelet transform or curvelet transform, etc). Now, our signal $f \in \Re^n$ is represented as $f = Dx$. Here, $D \in \Re^{n \times d}$. In other words, the non-sparse signal f is transformed into the sparse coefficients x in dictionary D. In the following section, we introduce shearlet transform as the sparsity dictionary.

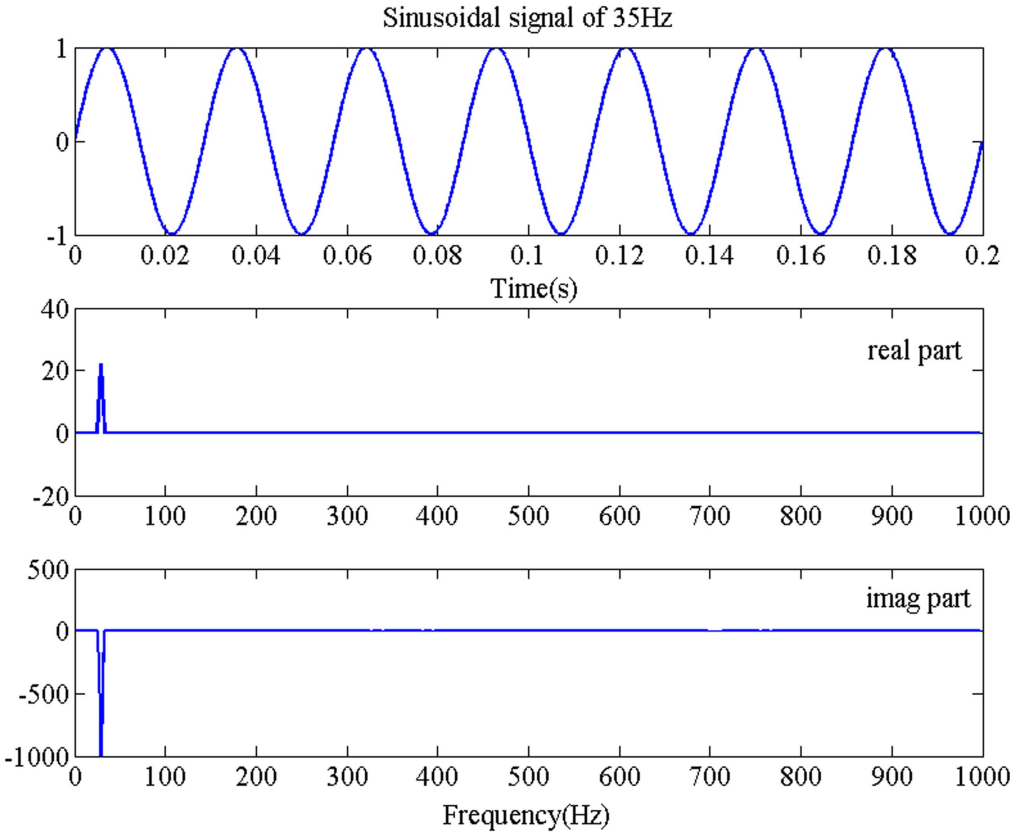

Figure 2. Sinusoidal signal and Fourier transform.

Introduction to shearlet transform

In the past several years, representation of bigger and higher-dimensional data sets have become of increasing concern. Wavelet transform has generated huge success in the image analysis and processing field, but has failed to represent high-dimensional anisotropic data, which has promoted the exploration of the anisotropic wavelet by researchers. To solve this problem, contourlets, brushlets, ridgetlets, and curvelets, etc have been widely applied in recent years, and the curvelet proposed by Candès and Donoho (2004) has achieved great success. This is the first and so far the only construction providing an essentially optimal approximation property for 2D piecewise smooth functions with discontinuities along C^2 curves. In this paper, a new discrete multi-scale sparse representation—shearlet transform (Labate and Kutyniok 2005, Guo *et al* 2005, Kutyniok *et al* 2011, Kittipoom *et al* 2012)—has been introduced. Shearlet transform is advantageous over classical wavelet transform as it provides information about the directionality within the image. Compared with curvelet transform, shearlet transform is easier to construct and has a simpler mathematical structure. Thus. the shearlet basis enables a more reliable transition from continuous to discrete.

In the 2D condition, the parabolic scaling matrix A_a and shear matrix S_s can be defined as follows:

$$A_a = \begin{pmatrix} a & 0 \\ 0 & \sqrt{a} \end{pmatrix},\ a \in R^+,\ S_s = \begin{pmatrix} 1 & s \\ 0 & 1 \end{pmatrix},\ s \in R, \tag{4}$$

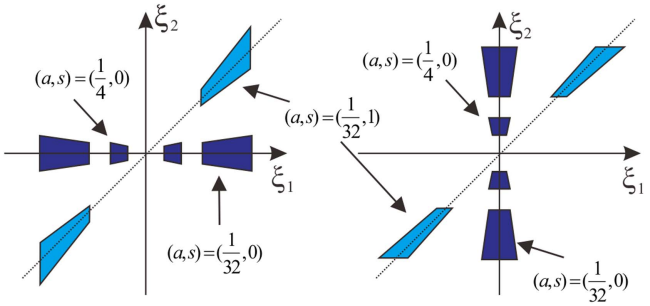

Figure 3. Frequency support of the horizontal shearlets (left) and vertical shearlets (right) for different values of a and s.

where a is the scaling parameter and s is the shearing parameter.

A shearlet system can be constructed by scaling, shearing, and translation of the continuous shearlet basis functions:

$$\varphi_{a,s,t}(x) := a^{-\frac{3}{4}}\varphi(A_a^{-1}S_s^{-1}(x-t)),\ a>0,\ s \in R,\ t \in R^2, \tag{5}$$

where t is the translation parameter. Then, continuous shearlet transform of an arbitrary function f is given by:

$$SH_\varphi f(a,s,t) = \langle f, \varphi_{a,s,t} \rangle. \tag{6}$$

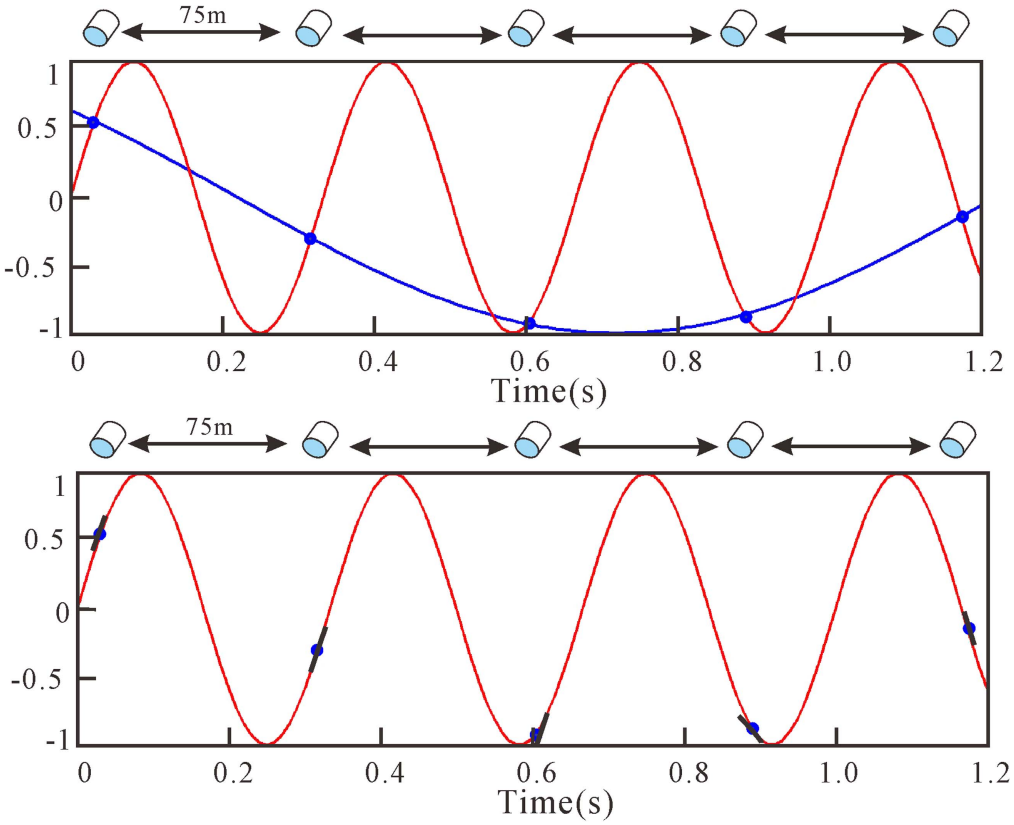

Figure 4. Single-channel versus multi-channel reconstruction, The single-channel reconstruction has only the amplitude information at the measuring position, and the sparse high-frequency sampling would cause serious aliasing. The multi-component reconstruction measures the amplitude and the gradient at the same position, so that the high-frequency wavefield can be reconstructed precisely.

Shearlet basis functions at various scales can be used to represent different frequency bands of data. Figure 3 shows the frequency tiling of shearlets. Low-scale shearlets capture a coarse representation of the input signals, while high-scale shearlets capture a fine representation of the input signals. Multi-directional shearlets represent curve-like data along certain directions making shearlet transform suitable to deal with anisotropic data.

Multi-channel interpolation using gradients

Seismic signals are point-recordings of curved seismic wavefronts. It is essential to select the direction-identifying anisotropic wavelets, so that the shearlet transform can represent the seismic signals effectively. So, a signal f could be represented as $f = S^{-1}x$, where S^{-1} is the inverse shearlet transform. Because the shearlet transform is redundant, the length of the shearlet coefficient vector exceeds dozens of times the signal. Therefore, in the sense of compressive sensing, the signal recovery problem turns into an estimate of a set shearlet coefficients x. We introduce compressed sensing into the seismic data reconstruction, and add a mask matrix $\boldsymbol{M}$ as the measurement matrix in the compressed sensing problem. When the elements in $\boldsymbol{M}$ are 0, the data is rejected; when the elements are 1, the data is accepted.

When the shearlet transform is combined with the iterative threshold method, the seismic data recovery problem can be induced to the following l_1 norm optimization problem:

$$\hat{x} = \arg \boldsymbol{min}_x \text{ subject to } \|y - MS^{-1}x\|_2 \leqslant \varepsilon. \tag{7}$$

The above constraint optimization problem could be replaced by unconstrained optimization problems according to Elad *et al* 2005:

$$\begin{cases} \hat{x}_\lambda = \arg \underset{x}{\boldsymbol{min}} \text{ subject to } \|y - MS^{-1}x\|_2 + \lambda \|x\|_1 \\ \hat{f} = S^{-1}\hat{x} \end{cases}. \tag{8}$$

The problem is transformed to reconstruct seismic data in the shearlet domain, and obtain a group of shearlet coefficients x under the minimum l_1 norm. These optimization problems depends on the Lagrange multiplier λ. The iterative thresholding technique based on the Landweber descent method (Vogel 2002) has been adopted. According to Deaubechies *et al* (2004):

$$x_{i+1} = T_\lambda(x_i + A^T(y - Ax_i)), \tag{9}$$

where $A = MS^{-1}$, and the soft threshold function $T_\lambda(x) : = \boldsymbol{sgn}(x) \cdot \boldsymbol{max}(0, |x| - |\lambda|)$.

The cooling method developed from equation (9) is a common strategy to solve large to extremely large scale problems (Herrmann and Hennenfent 2008). With this method, sparsity is first emphasized by setting a large λ, then the Lagrange multiplier λ decreases to include more transform coefficients into the solution interval. The above

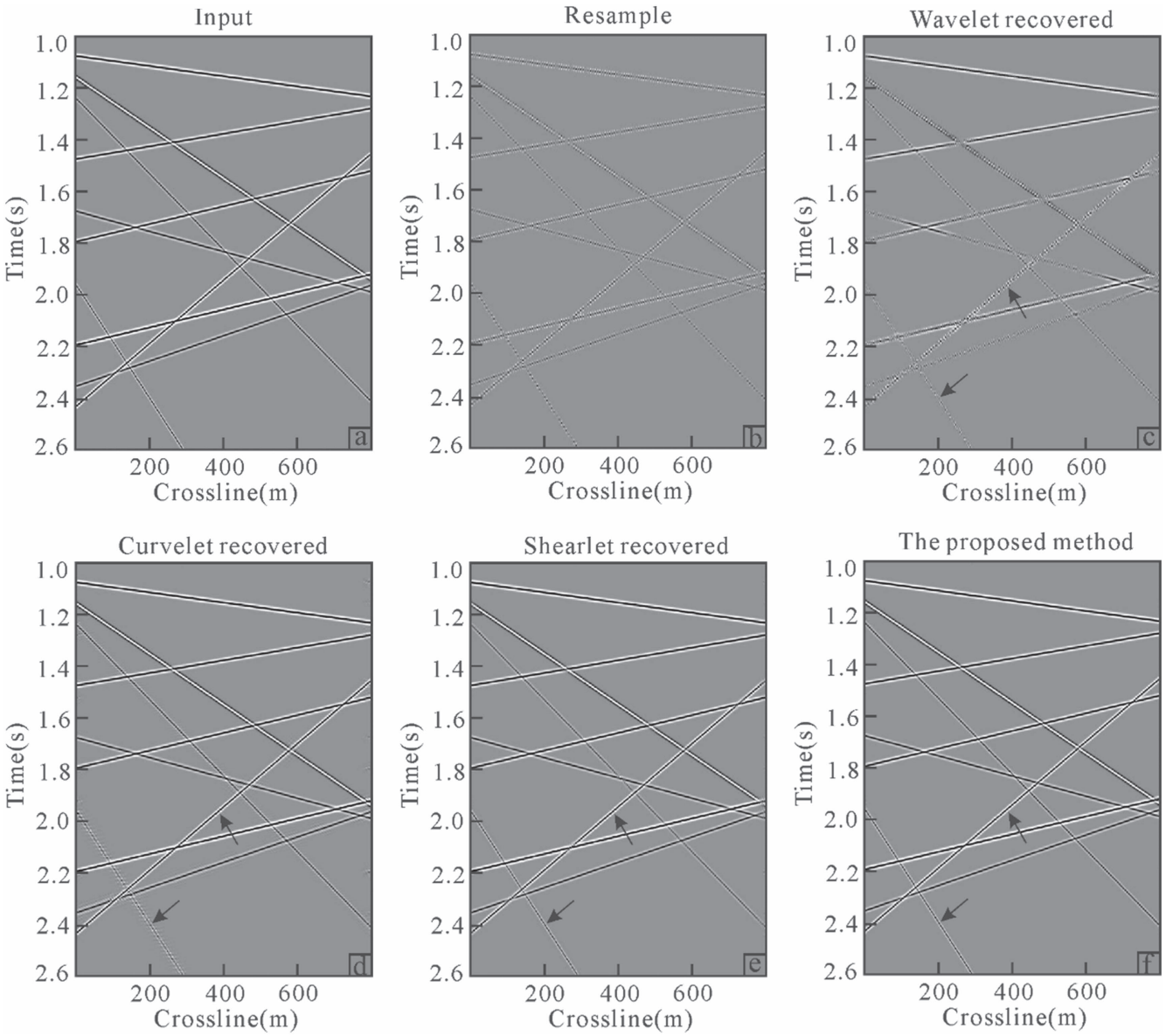

Figure 5. Example with simple synthetics: close-up of the whole data set in the *t-y* domain. (a) Total pressure sampled at 25 m; (b) input pressure sampled at 100 m; (c) pressure reconstructed by wavelet interpolator; (d) pressure reconstructed by curvelet interpolator; (e) pressure reconstructed by shearlet interpolator; (f) pressure reconstructed by using shearlet sparse constraint also having as input the crossline gradients at the samples positions.

solution method constitutes the basis of multi-component seismic data reconstruction.

In the multi-component marine data acquisition, the acceleration information (particle acceleration vector) is used to supplement the pressure data, and the equation of motion discloses the proportional relation between the pressure $\boldsymbol{P}$ and the acceleration under the acoustic assumption:

$$\Delta \boldsymbol{P} = -\rho \boldsymbol{\alpha}, \tag{10}$$

where ρ is the density of the medium. In the direction of the inline and crossline, we have:

$$\frac{\partial \boldsymbol{P}}{\partial x} = -\rho \dot{V}_x \text{ and } \frac{\partial \boldsymbol{P}}{\partial y} = -\rho \dot{V}_y, \tag{11}$$

where V_x and V_y are the velocity in the direction of the inline and crossline, respectively, and the dot above the scalar denotes the time gradient. A multi-component seismic acquisition measuring the three components of the velocity vector, therefore acquires the pressure field and its spatial derivatives. Compared with single-component seismic exploration, the multi-component seismic data acquires richer seismic wavefield information, which may improve the resolution of deep and fine scale structures such as faults.

In figure 4, the sinusoidal function is used for the reconstruction of five streamers whose sampling interval is 75 m in the crossline direction. As the sampling interval is very sparse, many sinusoidal functions are able to fit the data, and such a single-channel reconstruction would cause the rather serious aliasing. By contrast, the multi-component seismic data reconstruction can reduce multiplicity and get the correct wavefield at the same sampling position in the case of

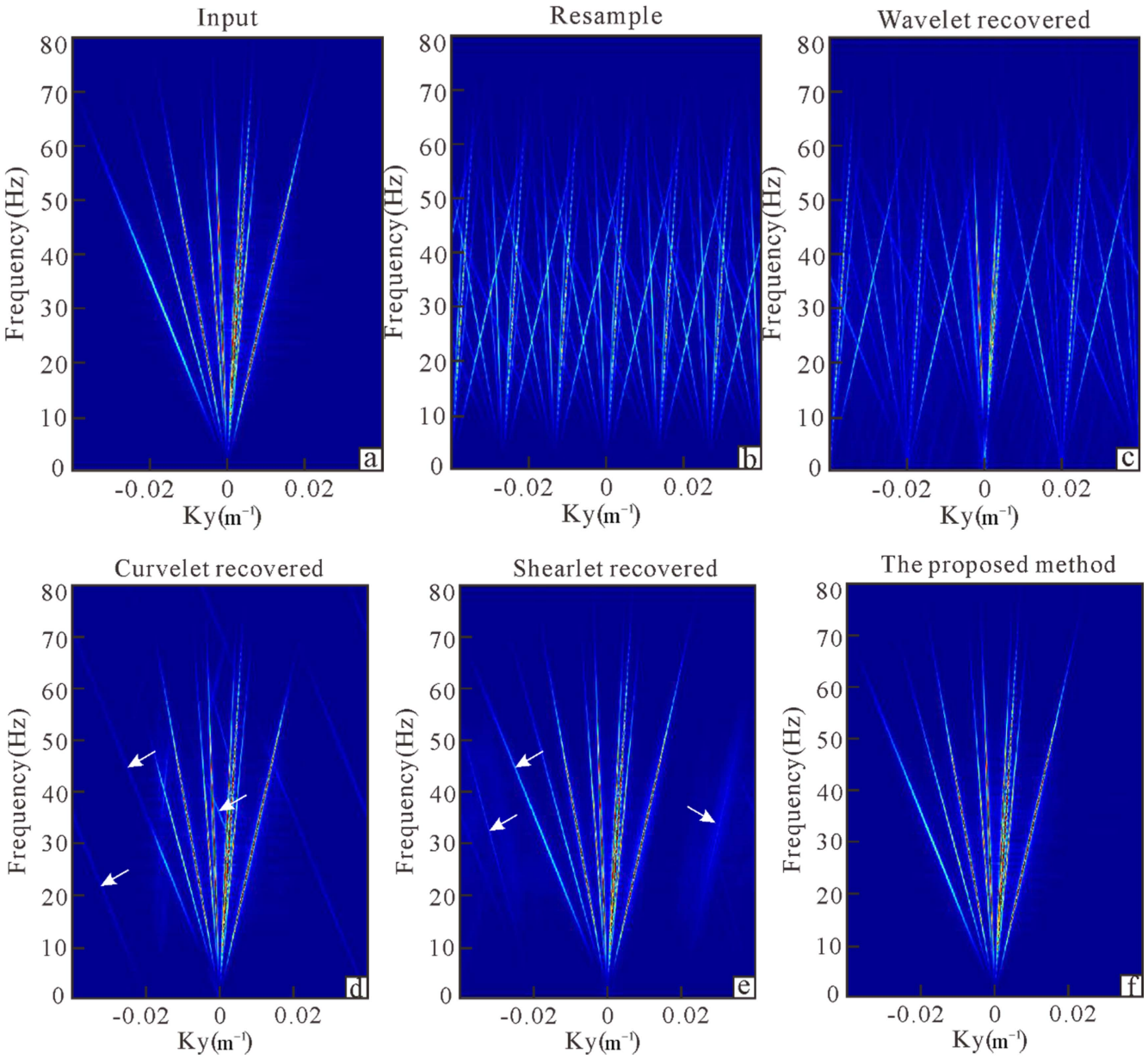

Figure 6. Example with simple synthetics: close-up of the *f-k* spectrum corresponding to figures 5(a)–(f).

gradient constraint. This may not always true, but shows the potential of multi-components in data reconstruction.

The pressure and crossline component of the particle-velocity measurements can be used as the constraint conditions for each other to provide the extra information for reconstruction. With pressure and its partial derivative along the crossline gradient obtained through the V_y measurements, they act as the input of the multi-component reconstruction. We carry out crossline wavefield reconstruction from multi-component seismic data by shearlet sparse constraint by:

$$\min_{x_p,x_v}\left\{\left\|\boldsymbol{P}-M\sum_{\text{trace}=1}^{n}\boldsymbol{S}^{-1}x_v\right\|_2+\left\|\dot{V}_y-M\frac{\partial\boldsymbol{S}^{-1}x_p}{\partial y}\right\|_2:\ \frac{\partial\boldsymbol{P}}{\partial y}=-\rho\dot{V}_y\right\},\tag{12}$$

where $\boldsymbol{P}$ is the pressure wavefield, $\dot{V}_y$ is the gradient data of the crossline velocity, M is the measurement matrix, and S^{-1} is the inverse shearlet transform. x_p and x_v represent a set of minimizing shearlet coefficients to reconstruct the pressure wavefield and the crossline particle-velocity wavefield, respectively. We adopted the multi-scale and multi-direction shearlet transform to represent the seismic data and produce the sparsest of the data. A method altering between the pressure field and the gradient wavefield were adopted to solve equation (12). First, the measured $\boldsymbol{P}$ and $\dot{V}_y$ were used as the input of the proposed method. We first recover a new $\boldsymbol{P}$ by threshold iteration based on the shearlet transform. Then, according to equation (11), $\dot{V}_y$ can be obtained by taking the derivative of $\boldsymbol{P}$. $\dot{V}_y$ can be used as the input to update a new $\dot{V}_y$ by threshold iteration. Put the updated $\dot{V}_y$ back into equation (11) and calculate $\boldsymbol{P}$ by integration. In this circulative iteration way, the gradient field provides the pressure

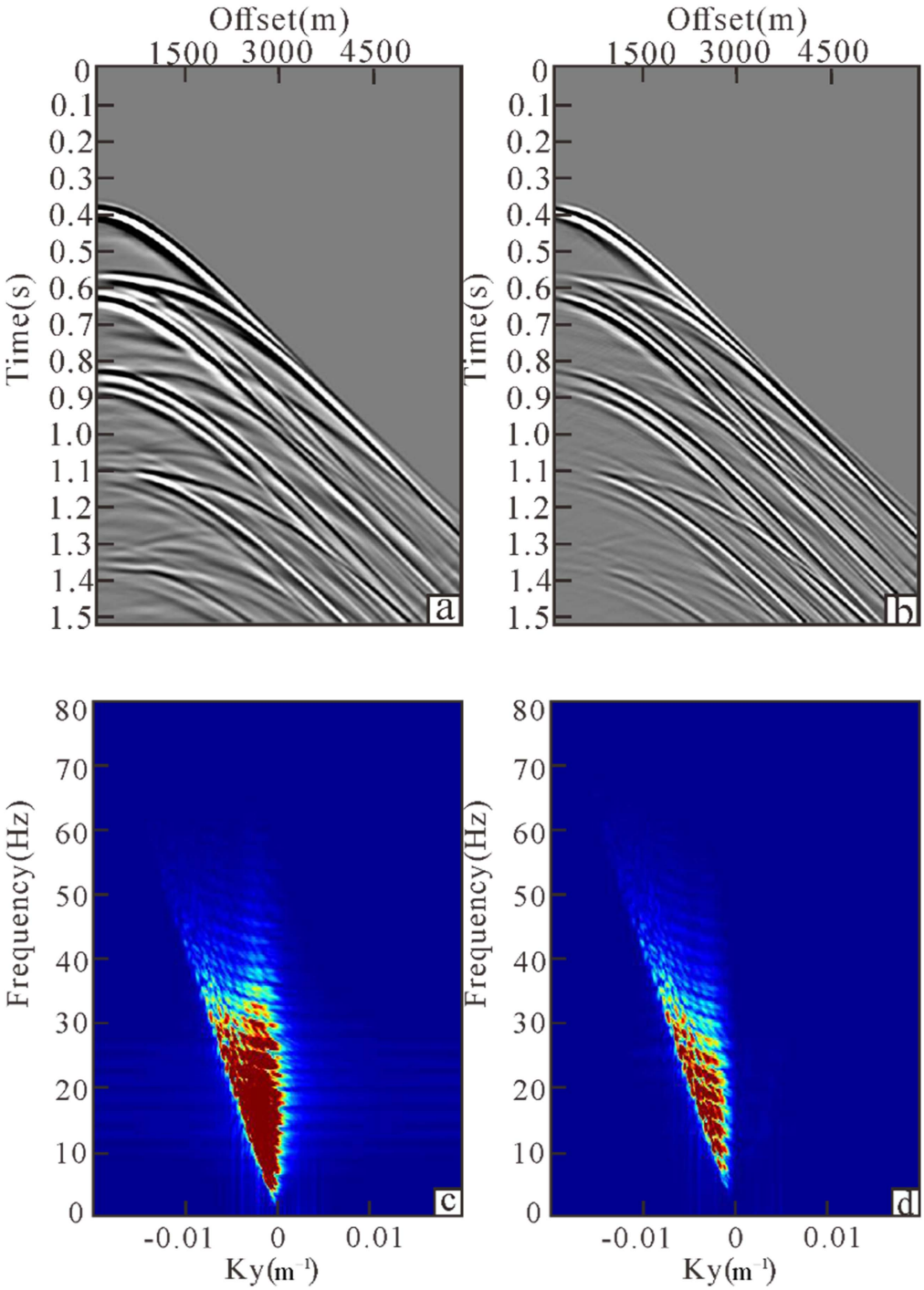

Figure 7. Overview of the synthetic data set: (a), (c) pressure and (b), (d) particle velocity, shown in the *t-x* and *f-k* domains, respectively.

wavefield reconstruction with the extra constraint conditions, which can reconstruct the severely aliased data effectively.

Altering iteration algorithm for minimizing equation (12)

1. Initialization:

Parameters: Iterations $\boldsymbol{N}$, thresholding factor λ_v, λ_p and tolerance ε_v, ε_p.
Initialize $P = 0$, $\dot{V}_y = 0$.
Set $\delta = \varepsilon^{1/(N-1)}$.

(Continued.)

2. Main iteration

For*i* = 1 to ***N*do**

Part A—Update $\boldsymbol{P}$ with $\dot{V}_y$ fixed:

—Calculate the residuals $Presp = M(\boldsymbol{P}_M - \boldsymbol{P})$

—Soft the shearlet coefficient of $\boldsymbol{P}$ component with the λ_p threshold and obtain $x_p = T_{\lambda_p}(x_p + S(\boldsymbol{P} + resp))$.

—Update P component by inverse shearlet transform $P = S^{-1}x_p$

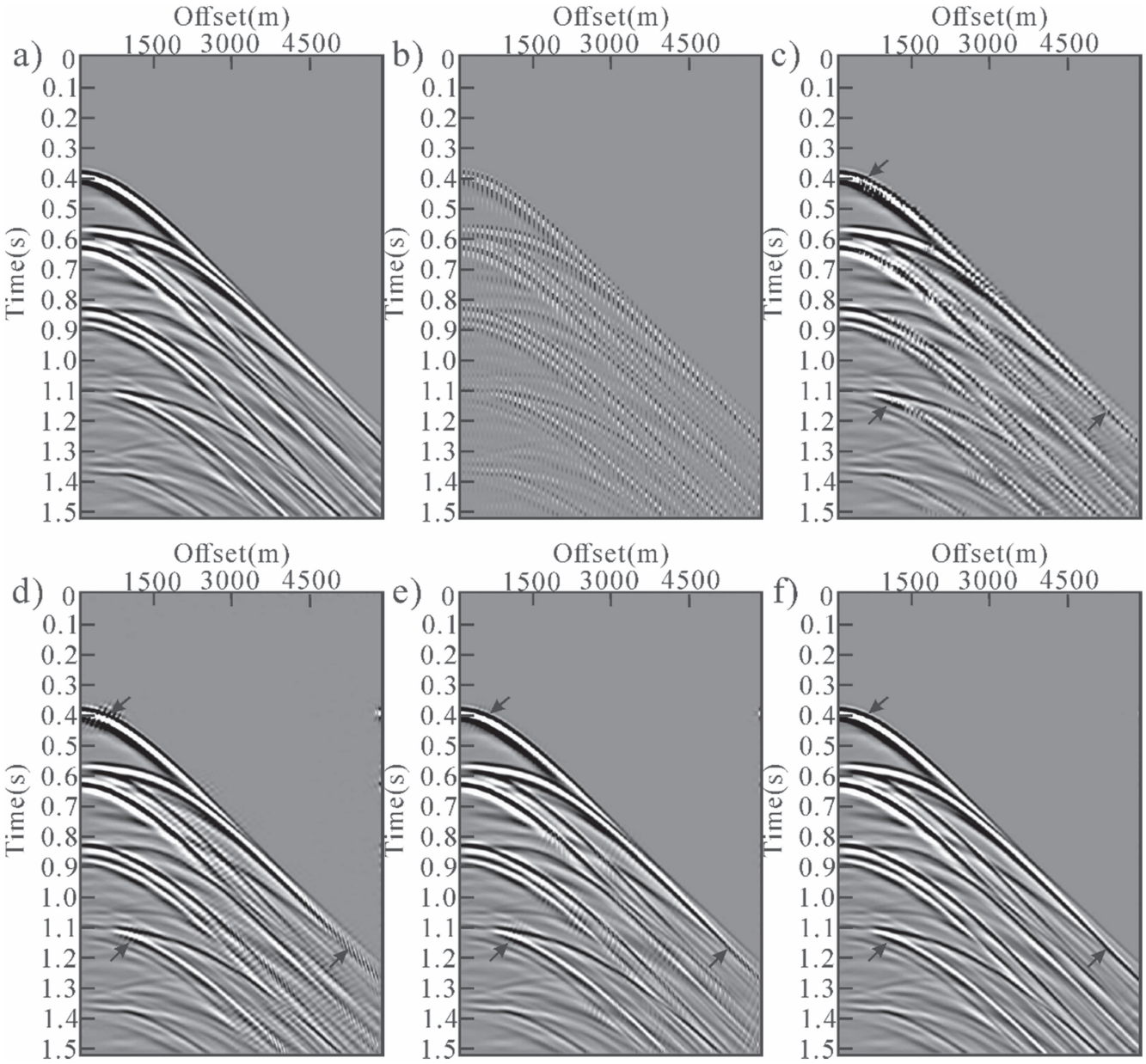

Figure 8. (a) Reference pressure data sampled at 25 m; (b) decimated input data sampled at 100 m; (c) pressure reconstructed by using a wavelet interpolator; (d) pressure reconstructed by using a curvelet interpolator; (e) pressure reconstructed by using a shearlet interpolator; (f) pressure reconstructed by using a shearlet sparse constraint also having as an input the crossline gradients at the samples' positions.

(Continued.)

Part B—Update $\dot{V}_y$ with $\boldsymbol{P}$ fixed:

—Calculate the residuals $resp = M(\dot{V}_M - \dot{V}_y)$

—Soft the shearlet coefficient of $\dot{V}_y$ component with the λ_v threshold and obtain $x_v = T_{\lambda_v}(x_v + S(\dot{V}_y + resv))$.

—Update $\dot{V}_y$ component by inverse shearlet transform $\dot{V}_y = S^{-1}x_v$.

Part C—Update the threshold λ_p and λ_v according to $\lambda_p = \delta \cdot \lambda_p$, $\lambda_v = \delta \cdot \lambda_v$.

3. If $\|P - MS^{-1}x_p\|_2 \leqslant \varepsilon_p \& \|\dot{V}_y - MS^{-1}x_v\|_2 \leqslant \varepsilon_v$ **finish**. **Else** return to **Step 2.**

4. Output: The reconstructed $\boldsymbol{P}$ and $\dot{V}_y$.

Numerical examples

Experiment on linear events

In order to test the effectiveness of our algorithm, we first synthesized ten linear events from different incidence directions. Figure 5(a) demonstrates the synthesized pressure wavefield. Then, we adopted wavelet transform (the discrete stationary wavelet transform used in this paper), curvelet transform, and shearlet transform to reconstruct the single-component seismic data, respectively, to verify the superiority of shearlet transform over other sparsifying transform. Then, we combined the shearlet transform and multi-component

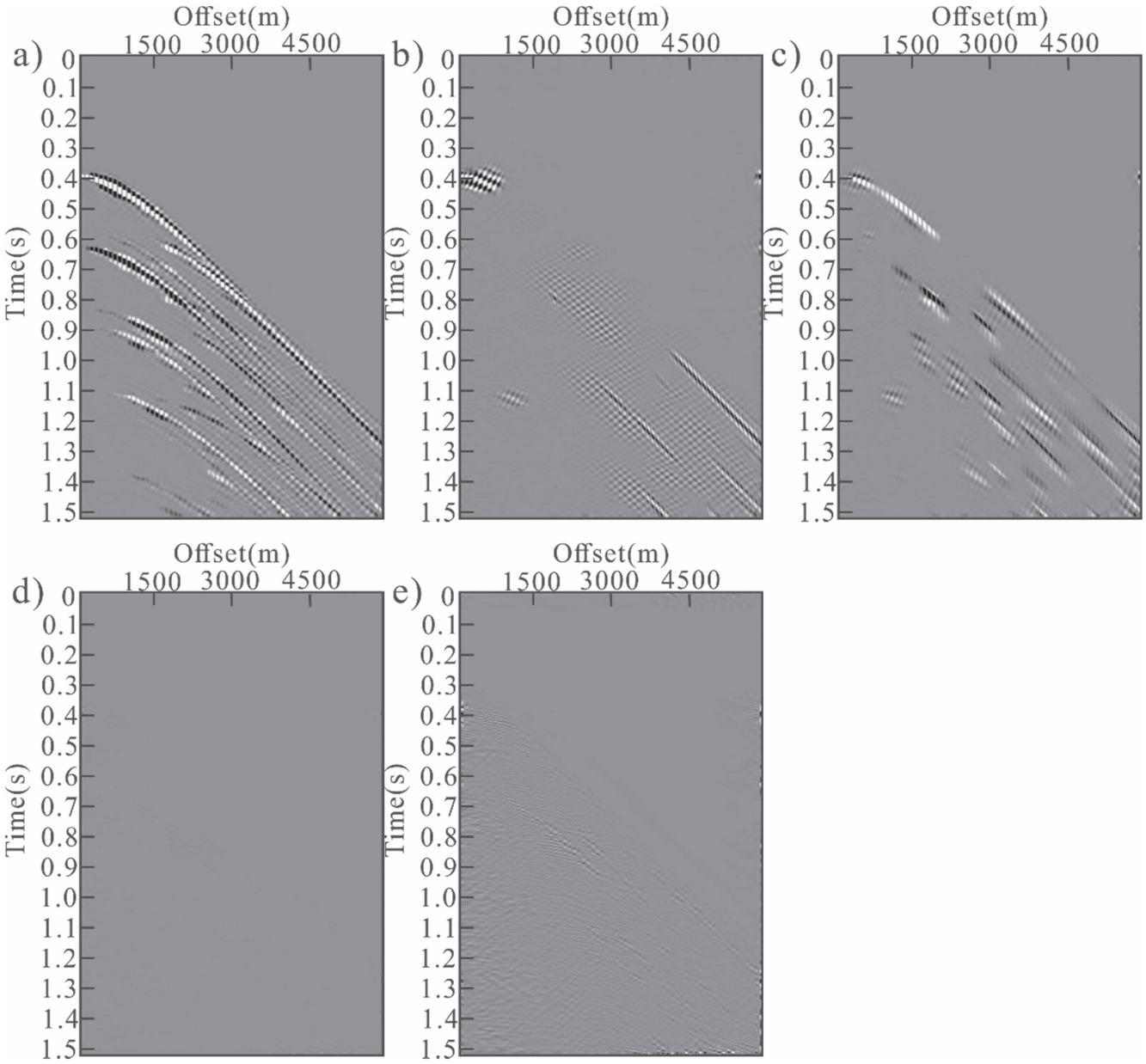

Figure 9. (a)–(d) errors in estimation of the pressure fields corresponding to figures 7(c)–(f); (e) the same with (d) but the amplitude gained ten times.

Table 1. Evaluation parameters of the synthetic data.

	PSNR/dB	SNR/dB
Wavelet interpolator	235.9457	4.5589
Curvelet interpolator	242.5709	11.1841
Shearlet interpolator	245.5156	14.1289
Shearlet with multi-component	267.3093	35.9225

seismic data for the wavefield reconstruction to make comparisons with the regular single-component method.

Figure 5(b) shows the input pressure sampled at 100 m. Figure 5(c) presents the seismic data reconstructed by a wavelet interpolator. The lost data have not been reconstructed effectively, meanwhile, the cross-section of events are in bad order. Though the curvelet interpolator (figure 5(d))

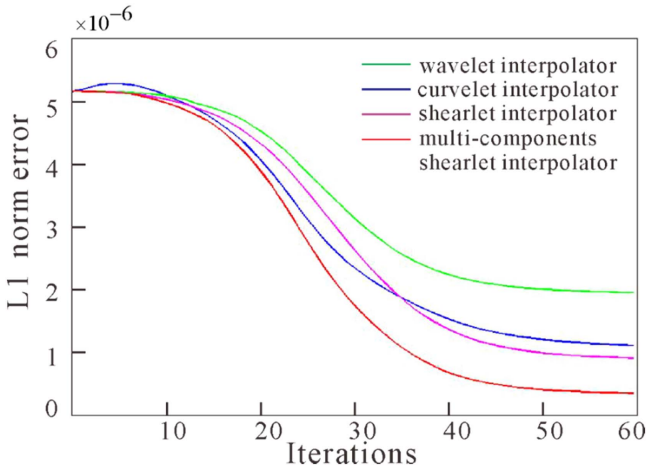

Figure 10. Convergence of the four interpolation methods.

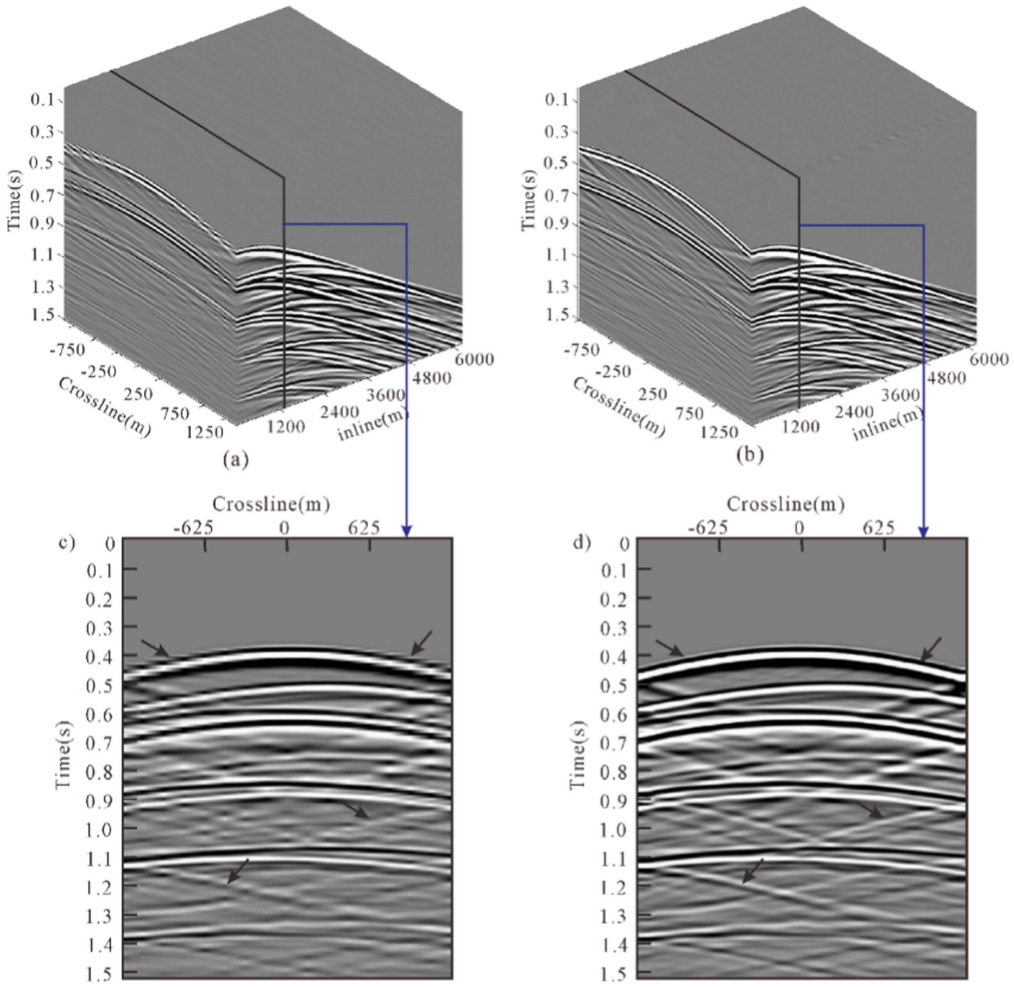

Figure 11. (a) Total wavefield before interpolation with 150 × 25 m spatial grid; (b) total reconstructed wavefield with 25 × 25 m spatial grid; (c), (d) close-ups of the crossline slices before and after reconstruction.

achieved better results than the wavelet interpolator, it shows poor performance in the big declivitous angle section indicated by the arrows. In the comparison of the three transforms, the shearlet interpolator achieved the most satisfactory results. When combining shearlet transform with the multi-component method, all the events are reconstructed perfectly, whose events are fairly smooth and clear.

Figure 6 display the *f-k* spectrum corresponding to figure 5. It is possible to visualize the impact of a spatial alias in the decimated data. The first order alias occurs for frequencies just above 15 Hz, and the order of the alias grows very significantly with frequency (figure 6(b)); figure 6(c) shows the *f-k* transform of the wavelet interpolator, and only frequencies up to 25 Hz are not aliased. Figure 6(d) shows the curvelet interpolator, and the aliasing was suppressed well but with spectrum leakage at high wavenumber (at the arrowhead). We can see how well the shearlet interpolator (figure 6(d)) performed and the energy distribution is more uniform compared with the curvelet transform. By contrast, the *f-k* spectrum reconstructed by the multi-component shearlet interpolator (figure 6(f)) basically conformed to the original *f-k* spectrum.

Experiment on curved events

To further illustrate the effectiveness of the proposed method on curved seismic arrival wavefronts, we synthesized a set of pressure data and the crossline gradient data sampled at 25 m spacing shown in figures 7(a) and (b). We resampled the data at 75% of the initial samplings period. The wavelet interpolator, curvelet interpolator, shearlet interpolator, and multi-component shearlet interpolator methods were adopted for data reconstruction. To compare the four methods, we introduced two parameters for evaluation, which are defined as follows:

(1) Signal to noise ratio (SNR):

$$\mathrm{SNR}=10\ln\frac{\|\boldsymbol{s}_0\|_2}{\|\boldsymbol{s}_1-\boldsymbol{s}_0\|_2},$$

where $\boldsymbol{s}_0$ is the original data and $\boldsymbol{s}_1$ is the reconstructed data.

(2) Peak signal to noise ratio (PSNR):

$$\mathrm{PSNR}=10\ln\frac{\boldsymbol{max}(\boldsymbol{s}_0)}{\sqrt{\sum(\boldsymbol{s}_1-\boldsymbol{s}_0)^2/M/N}},$$

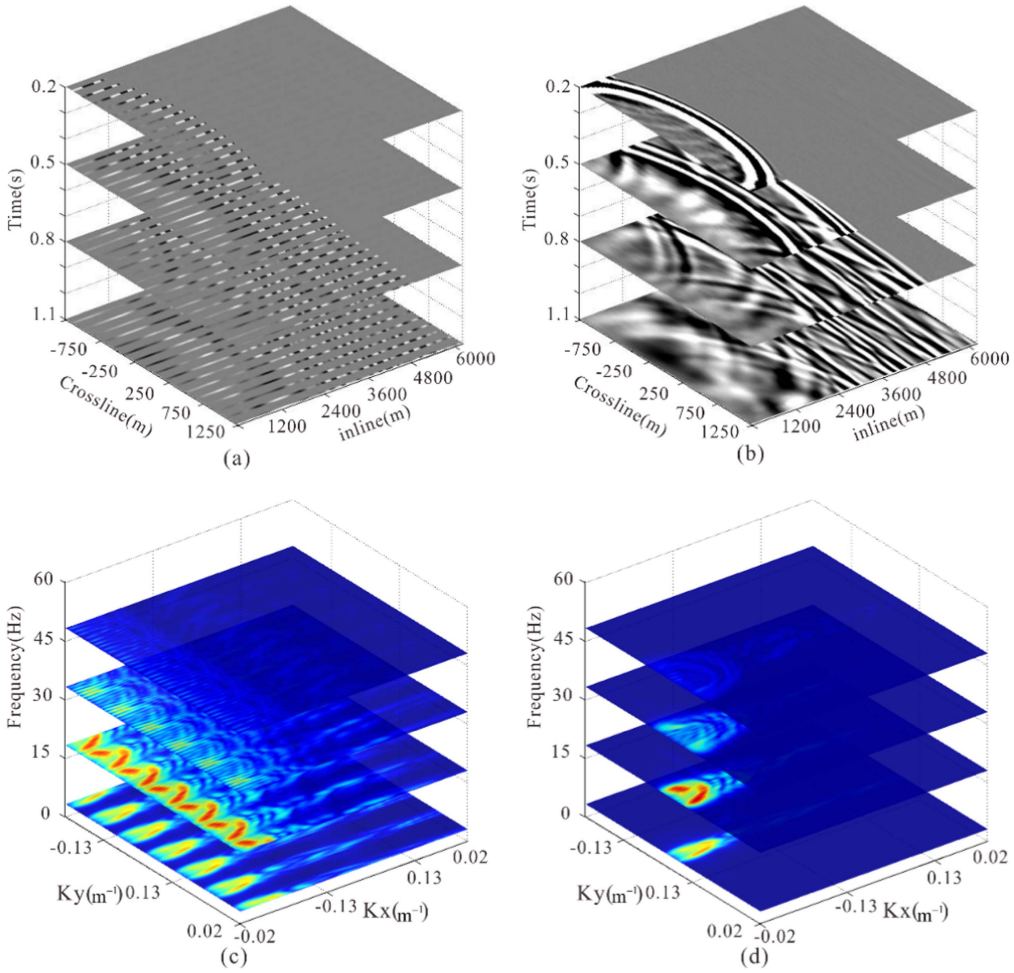

Figure 12. (a) Total wavefield before interpolation with 150 × 25 m spatial grid and time slice at 0.2 , 0.5 , 0.8, and 1.1 s; (b) total reconstructed wavefield by using a shearlet interpolator by multi-components with a 25 × 25 m spatial grid; (c), (d) the f-k_x-k_y transform of (a) and (b).

where M is the number of data rows, and N is the number of data columns.

Figures 8(a), (b) display the reference pressure data sampled at 25 m and the decimated input data sampled at 100 m. Figure 8(c) presents the result of wavelet interpolator (SNR =4.5589 dB), both the continuity of events and the reconstruction precision are abysmal. Figure 8(d) illustrates the result of the curvelet interpolator (SNR = 11.1841 dB), which is much better than that of wavelet interpolator, but failed in restoring the section of the big curvature (0.4 s). Figure 8(e) shows the result of the shearlet interpolator (SNR = 14.1289 dB), which is improved among the three transform reconstructions; it settles the problem of bad reconstruction effect at the sections of the big curvature with the curvelet interpolator. Figures 8(c)–(e) demonstrate that the shearlet transform has the optimal representation of seismic data among the three transforms. Figure 8(f) demonstrates the result of the multi-component seismic data by shearlet sparse constraint (SNR = 35.9225 dB); the reconstruction precision has been improved with the gradient constraint and obtains a nice continuity along the events. The evaluation parameters in table 1 also demonstrate that the multi-component method is remarkably better than that of the single-component reconstruction.

Figures 9(a)–(d) are the corresponding error profiles of figures 8(c)–(f). By comparing the error profiles of the three transforms, the error of wavelet interpolator (figure 9(a)) contains substantial energy; figure 9(b) depicts the reconstruction error by the curvelet interpolator. Here, the residual energy appears out of the missing signals area, which displays its imprecise representation of seismic data. In figure 9(c), we see minor residual energy at the error profile, and the residual energy gathers along the events position, which indicates the more precise representation of seismic data by shearlet transform than that of the wavelet or curvelet transform. The error profile energy is extremely weak by the proposed method (figure 9(d)), and little residual energy can be seen even by scaling a factor of ten in figure 9(e). The results shown in figure 9 confirm the favorable effect using the crossline gradient constraint.

Figure 10 shows the iterative convergence curves of the four reconstruction methods used in the curve events test with a total of 60 iterations. It is clear from the figure that the wavelet transform has the lowest convergence rate and the

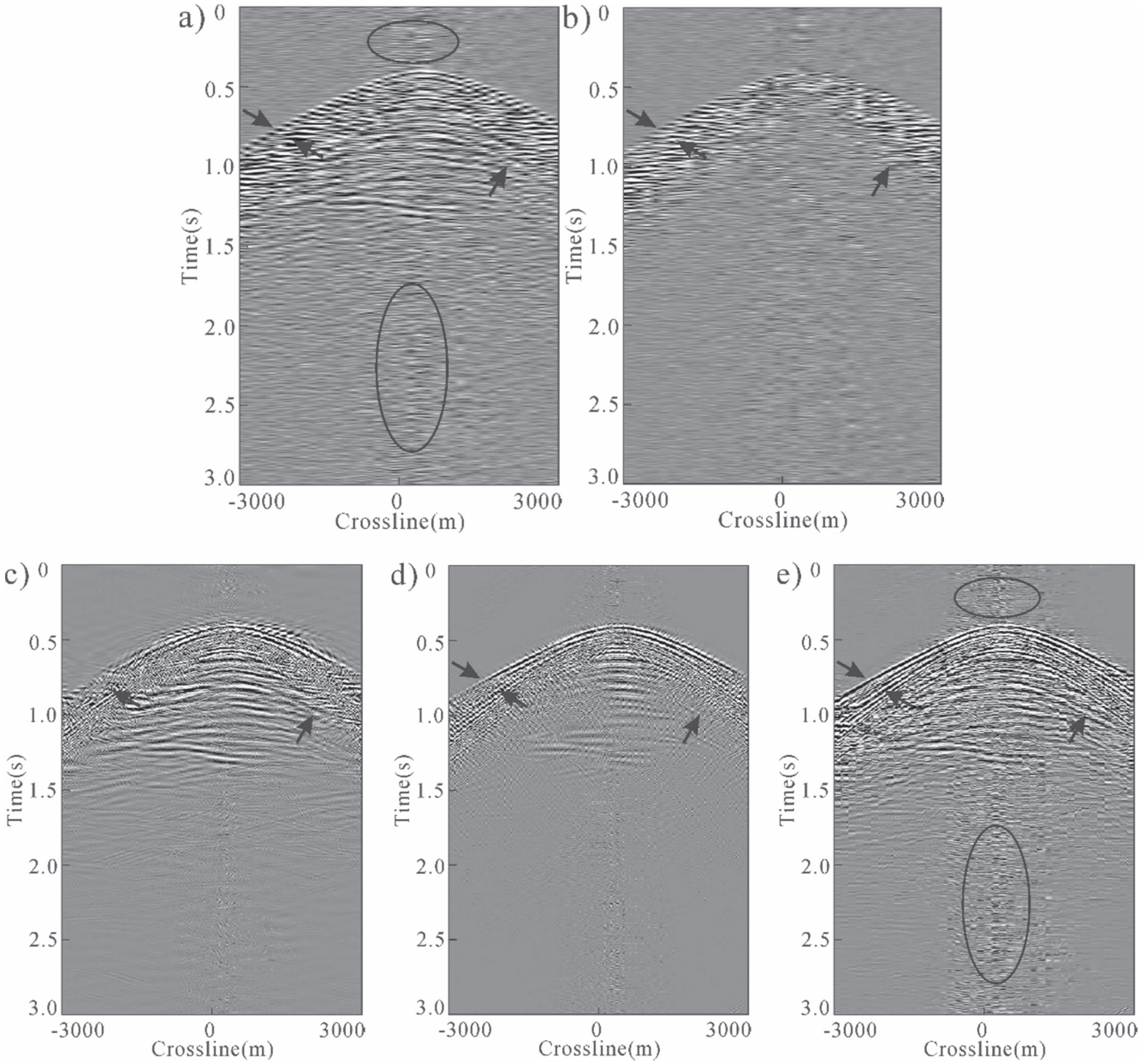

Figure 13. Example of field data. (a), (b) Total pressure and the corresponding gradients, sampled at 150 m; (c) pressure reconstructed by using a curvelet interpolator; (d) pressure reconstructed by using a shearlet interpolator; (e) pressure reconstructed by using a multi-channel shearlet also having as an input the crossline gradients at the samples' positions.

largest convergence error. The curvelet transform acquires a better convergence rate than the shearlet transform does in the first 35 iterations, but its convergence error becomes bigger than that of the shearlet transform as the iterations increase. The reason for this is that the shearlet transform usually exhibits seven times the redundancy of the curvelet transform, which leads to the shearlet possessing a higher solution precision and low convergence speed. As a result, with fewer iterations and fewer coefficients included in the solution, the curvelet transform achieved a better reconstruction result. However, as the number of iterations increases and more coefficients are included into the solution interval, the shearlet transform achieved a better reconstruction result, while the multi-component method achieved the fastest convergence rate and lowest error benefiting from the additional component constraint.

Realistic 3D data test

To test the proposed method on a highly aliased 3D data set, we synthesized a 3D data set which consisted of 17 streamers with a 150 m crossline spacing and 25 m inline spacing. As we already well sampled in the inline direction, we just carried out the crossline reconstruction and reconstructed the 150×25 m wavefield into the 25×25 m wavefield. Figures 11(a) and (b) demonstrate the wavefields before and after the reconstruction. Close-ups of the crossline slices are shown in figures 11(c) and (d). Obviously, the reconstructed

profile exhibits better continuity and clarity, especially in the complex structure and curved events indicated by the arrows.

Figures 12(a) and (b) show four time slices at $t = 0.2$, 0.5, 0.8, and 1.1 s before and after the reconstruction. In figure 12(a), the crossline data are rather sparse, so the details cannot be identified. Figure 12(b) shows the wavefield time slice after reconstruction. The event has been well recovered and the detailed information has been demonstrated clearly. The sparse sampling wavefield f-k_x-k_y transform generates severely spatial aliasing, and the order of alias grows significantly with frequency. Figure 12(d) shows the recovery wavefield f-k_x-k_y transform, the very successful dealiasing impact achieved by the proposed method compared to figure 12(c).

Field data test

To illustrate the effect of this method on the field data, we selected the marine ocean bottom cable data for the test. Figures 13(a) and (b) display the pressure data and the corresponding V_y, which contains 40 traces in the crossline direction at 150 m spacing. The sparse wavefield makes it difficult to track the events. Figures 13(c) and (d) show the results of the single-component interpolator by curvelet and shearlet, respectively. Obviously, the curvelet interpolator kept more energy but the events exhibit normally with poor continuity, while the shearlet interpolator kept less energy but the events were smoother and finer. In figure 13(e) we can observe that the most significant information present in the pressure wavefield shows better continuity and resolution.

We can see that the multi-component shearlet interpolator seems to boost noise in the shallow and deep area. In theory, the iterative threshold method could attenuate the random noise, while we could find that the noise showed low-amplitude and regular continuity from the circled area in figures 13(a) and (e). These continuity signals could not be removed like random noise, and could be involved in reconstruction. So, the reconstructed data seems like noise.

Conclusions

Driven by the compressed sensing theory, we introduced the shearlet transform into the seismic data reconstruction problem. Due to excellent sparsity and directivity of a shearlet, it can represent the seismic data well without linear event assumptions and normal moveout correction pretreatments. On this basis, we developed multi-component seismic data reconstruction, using both the crossline pressure and crossline gradients as inputs. In this way, our scheme achieves satisfactory anti-aliasing and fairly high-quality recovery precision. Numerical examples demonstrate that the proposed method could effectively reconstruct the dealiased crossline wavefield even with a small number of samples. Currently, our method is aimed only at 2D crossline slice reconstruction. In the future, we will introduce 3D shearlet transform into the multi-component seismic data reconstruction, and a real 3D multi-component seismic data reconstruction is our next target.

Acknowledgments

We thank the ShearLab for sharing their codes on the Internet (www.shearlab.org). This research is supported by the Major Projects of the National Science and Technology of China (Grant No. 2016ZX05026-002-003), National Natural Science Foundation of China (41374108), and Graduate Innovation Fund of Jilin University (No. 2017090). The authors would like to thank the China National Offshore Oil Company for providing field data.

References

Candès E J and Donoho D L 2004 New tight frames of curvelets and optimal representations of objects with piecewise C^2 singularities *Comm. Pure Appl. Math.* **57** 219–66

Candès E J and Romberg J K 2005 Signal recovery from random projections *Proc. SPIE* **5674** 76–86

Candès E J and Wakin M B 2008 An introduction to compressive sampling *IEEE Signal Process. Mag.* **25** 21–30

Canning A and Gardner G H F 2012 Regularizing 3D data sets with DMO *Geophysics* **61** 1103–14

Chemingui N and Biondi B 1996 Handling the irregular geometry in wide-azimuth surveys *SEG Technical Program Expanded Abstracts 1996* (Tulsa, OK: Society of Exploration Geophysicists) pp 32–35

Daubechies I, Defrise M and Mol C D 2004 An iterative thresholding algorithm for linear inverse problems with a sparsity constrains *Commun. Pure Appl. Math.* **57** 1413–57

Donoho D L 2006 Compressed sensing *IEEE Trans. Inf. Theory* **52** 1289–306

Elad M *et al* 2005 Simultaneous cartoon and texture image inpainting using morphological component analysis (MCA) *Appl. Comput. Harmon. Anal.* **19** 340–58

Fomel S and Liu Y 2010 Seislet transform and seislet frame *Geophysics* **75** V25–38

Gulunay N and Chambers R E 1996 Unaliased f-k domain trace interpolation (UFKI) *SEG Technical Program Expanded Abstracts 1996* (Tulsa, OK: Society of Exploration Geophysicists) pp 1461–4

Guo K, Kutyniok G and Labate D 2005 Sparse multidimensional representations using anisotropic dilation and shear operators *Int. Conf. on the Interaction Between Wavelets and Splines (Athens, GA)* pp 189–201

Herrmann F J and Hennenfent G 2008 Non-parametric seismic data recovery with curvelet frames *Geophys. J. Int.* **173** 233–48

Herrmann F J, Moghaddam P and Stolk C C 2008a Sparsity- and continuity-promoting seismic image recovery with curvelet frames *Appl. Comput. Harmon. Anal.* **24** 150–73

Herrmann F J, Wang D and Verschuur D J 2008b Adaptive curvelet-domain primary-multiple separation *Geophysics* **73** A17–21

Labate D and Kutyniok G 2005 Sparse multidimensional representation using shearlets *Proc. SPIE* **5914** 254–62

Liu B and Sacchi M D 2004 Minimum weighted norm interpolation of seismic records *Geophysics* **69** 1560–8

Kutyniok G, Shahram M and Zhuang X 2011 ShearLab, A rational design of a digital parabolic scaling algorithm *SIAM J. Imag. Sci.* **5** 1291–332

Kittipoom P, Kutyniok G and Lim W Q 2012 Construction of compactly supported shearlet frames *Constr. Approx.* **35** 21–72

Posthumus B J 1993 Deghosting using a twin streamer configuration *Geophys. Prospect.* **41** 267–86

Robertsson J *et al* 2008 On the use of multicomponent streamer recordings for reconstruction of pressure wavefields in the crossline direction *Geophysics* **73** A45–9

Schlumberger Technology Corp. 2004 Method and system for reducing effects of sea surface ghost contamination in seismic data *US Patent Specification* 6775618

Mobil Oil Corp. 1984 Pressure and velocity detectors for seismic exploration *US Patent Specification* 4486865

Shell Oil Co. 1984 Marine seismic system *US Patent Specification* 4437175

Spitz S 1991 Seismic trace interpolation in the *F-X* domain *Geophysics* **56** 785–94

Vassallo M *et al* 2010 Crossline wavefield reconstruction from multicomponent streamer data: Part 1—multichannel interpolation by matching pursuit (MIMAP) using pressure and its crossline gradient *Geophysics* **75** WB53–67

Vogel C R 2002 *Computational Methods for Inverse Problems* (Philadelphia, PA: Society for Industrial and Applied Mathematics)

Xue Z, Zhu H and Fomel S 2017 Full-waveform inversion using seislet regularization *Geophysics* **82** A43–9